BIOCHEMISTRY
including biophysical chemistry & molecular biology
Article

Biochemistry **2010,** *49,* 4103–4115 4103
DOI: 10.1021/bi100066j

RNA Aptamers as Conformational Probes and Regulatory Agents for Plasminogen Activator Inhibitor-1†

Jeppe B. Madsen,[‡,§] Daniel M. Dupont,[§,∥] Thomas B. Andersen,[‡,§,∥] Anne F. Nielsen,[§] Lu Sang,[‡,§,∥] Ditte M. Brix,[§] Jan K. Jensen,[‡,§] Thomas Broos,[§] Maarten L. V. Hendrickx,[§] Anni Christensen,[‡,§] Jørgen Kjems,[‡,§,∥] and Peter A. Andreasen*[,‡,§,∥]

[‡]*Danish-Chinese Center for Proteases and Cancer, and* [§]*Department of Molecular Biology, Aarhus University, 10C Gustav Wieds Vej, 8000 Aarhus C, Denmark, and* [∥]*Interdisciplinary Nanoscience Center (iNANO), Aarhus University, C. F. Møllers Allé 3, 8000 Aarhus C, Denmark*

Received January 15, 2010; Revised Manuscript Received March 24, 2010

ABSTRACT: The hallmark of serpins is the ability to undergo the so-called "stressed-to-relaxed" switch during which the surface-exposed reactive center loop (RCL) becomes incorporated as strand 4 in central β-sheet A. RCL insertion drives not only the inhibitory reaction of serpins with their target serine proteases but also the conversion to the inactive latent state. RCL insertion is coupled to conformational changes in the flexible joint region flanking β-sheet A. One interesting serpin is plasminogen activator inhibitor-1 (PAI-1), a fast and specific inhibitor of the serine proteases tissue-type and urokinase-type plasminogen activator. Via its flexible joints' region, native PAI-1 binds vitronectin and relaxed, protease-complexed PAI-1 certain endocytosis receptors. From a library of 35-nucleotides long 2′-fluoropyrimidine-containing RNA oligonucleotides, we have isolated two aptamers binding PAI-1 by the flexible joint region with low nanomolar K_D values. One of the aptamers exhibited measurable binding to native PAI-1 only, while the other also bound relaxed PAI-1. While none of the aptamers inhibited the antiproteolytic effect of PAI-1, both aptamers inhibited vitronectin binding and the relaxed PAI-1-binding aptamer also endocytosis receptor binding. The aptamer binding exclusively to native PAI-1 increased the half-life for the latency transition to more than 6 h, manyfold more than vitronectin. Contact with Lys124 in the flexible joint region was critical for strong inhibition of the latency transition and the lack of binding to relaxed PAI-1. We conclude that aptamers yield important information about the serpin conformational switch and, because they can compete with high-affinity protein−protein interactions, may provide leads for pharmacological intervention.

The distinguishing feature of proteins of the serpin superfamily is their ability to undergo the so-called stressed-to-relaxed conformational change, a transition mainly consisting of the insertion of the solvent-exposed reactive center loop (RCL[1]) as strand 4 of central β-sheet A (Figure 1). Most serpins are serine protease inhibitors, and the stressed-to-relaxed transition drives the serpin inhibitory mechanism. At the initial encounter between a serpin and its target protease, a so-called Michaelis complex is formed, in which the protease active site binds noncovalently to the reactive center peptide (P1−P1′) bond. The protease active site attacks the serpin's P1−P1′ peptide bond, leading to formation of an acyl−enzyme intermediate, in which the carboxyl group of the P1 residue is attached by an ester bond to the hydroxyl group of the active site Ser. The breakage of the P1−P1′ bond allows stabilization of the serpin by RCL insertion, leading to translocation of the protease to the opposite pole of the serpin. Upon translocation of the protease, a deformation of the active site prevents the completion of the catalytic cycle, resulting in the formation of a stable, covalent complex between the serpin and the protease (for reviews, see refs *1* and *2*). Under some conditions, complex formation is abortive and the P1−P1′ bond is cleaved without complex formation, termed serpin substrate behavior. In the serpins plasminogen activator inhibitor-1 (PAI-1) and antithrombin, the RCL can insert into β-sheet A without cleavage of the reactive center peptide bond. This change is termed the latency transition. Concomitantly with RCL insertion, β-strands 3A, 2A, and 1A are pushed toward α-helices D and E (Figure 1), which thereby shift conformation. The area comprising these helices and connecting loops is termed the flexible joints' region (for reviews, see refs *2* and *3*).

The serpin PAI-1 is a fast and specific inhibitor of both tissue-type plasminogen activator (tPA) and urokinase-type plasminogen activator (uPA), rendering it the primary physiological inhibitor of activation of the zymogen plasminogen to plasmin. The active serine protease plasmin can degrade substrates such as fibrin and other extracellular proteins (for a review, see ref *4*). Besides the

†This work was supported by the Danish National Research Foundation (26-331-6), the Danish Cancer Society (DP 07043 and DP 08001), the Danish Research Agency (272-06-0518), the Novo-Nordisk Foundation (R114-A11382), and the Danish Cancer Research Foundation.

*To whom correspondence should be addressed. Phone: +45 8942 5080. E-mail: pa@mb.au.dk.

[1]Abbreviations: AINBD, *N*-{[2-(iodoacetoxy)ethyl]-*N*-methyl}amino-7-nitrobenz-2-oxa-1,3-diazole; ATF, amino-terminal fragment of uPA; bis-ANS, 4,4′-dianilino-1,1′-bisnaphthyl-5,5′-disulfonic acid; ENU, ethylnitrosourea; EMSA, electrophoretic mobility shift assay; HBS, HEPES-buffered saline [30 mM HEPES and 135 mM NaCl (pH 7.4)]; LRP-1A, low-density lipoprotein receptor-related protein-1A; NBD, nitrobenz-2-oxa-1,3-diazole; PAI-1, plasminogen activator inhibitor-1; PBS, phosphate-buffered saline [10 mM sodium phosphate (pH 7.4) and 140 mM NaCl]; PDB, Protein Data Bank; S-2444, pyro-Glu-Gly-Arg-*p*-nitroanilide; RCL, reactive center loop; RU, response units; SELEX, Systematic Evolution of Ligands by Exponential Enrichment; SPR, surface plasmon resonance; uPA, urokinase-type plasminogen activator; uPAR, urokinase-type plasminogen activator receptor; VLDLR, very low-density lipoprotein receptor; wt, wild type.

Published on Web 04/13/2010

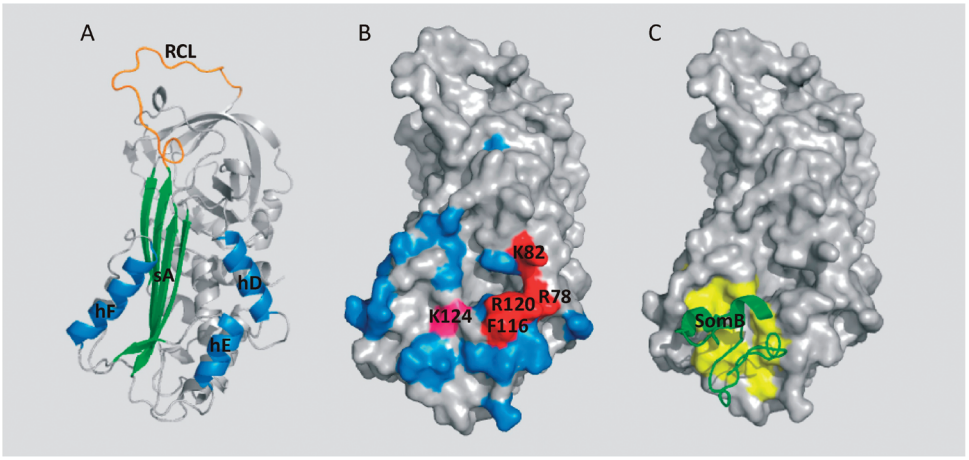

FIGURE 1: Structural features of PAI-1. (A) Ribbon presentation of the structure of PAI-1 in the active conformation (*60*) (PDB entry 1B3K). The RCL is colored orange and β-sheet A green, and α-helices D−F are colored blue. (B) Surface presentation of the same setup as shown in panel A with the residues tested for involvement in the binding of PAI-1 to paionap-5 and paionap-40 highlighted. Substitution of residues colored red (Arg78, Lys82, Phe116, and Arg120) with Ala resulted in no detectable binding, as determined by SPR analysis. The Lys124 colored pink was implicated in binding of paionap-40 but was of no importance for the binding of paionap-5. Substitution of residues colored blue (Lys71, Tyr81, Arg103, Gln109, Met112, Pro113, Arg117, Glu123A, Gln125, Arg133, Phe136, His145, Lys147, Asn152, Lys156, Trp177, Gln321, and Met356) with Ala had no measurable effect on binding of any of the aptamers. Residues colored gray were not tested for binding to the aptamers. (C) Surface representation of the structure of the PAI-1−somatomedin B complex (*53*) (PDB entry 1OC0), with somatomedin B colored green and somatomedin B-binding residues on PAI-1, as determined by site-directed mutagenesis (*21*), colored yellow. The figures were constructed with PyMol (*The PyMOL Molecular Graphics System*, version 1.2r3pre, Schrödinger, LLC).

plasminogen activators, PAI-1 also exhibits a high affinity for the protein vitronectin and endocytosis receptors of the low-density lipoprotein receptor family, like low-density lipoprotein receptor-related protein-1A (LRP-1A) and very low-density lipoprotein receptor (VLDLR) (for reviews, see refs *2* and *5*). Both vitronectin and the endocytosis receptors bind the flexible joint region. Vitronectin binds native PAI-1 with a low nanomolar K_D, while the affinity of RCL-inserted PAI-1 for vitronectin is ~100-fold lower. PAI-1−protease complexes bind with higher affinity to the endocytosis receptors as compared to free PAI-1 (*6*−*8*). This interaction allows the receptors to clear uPA−PAI-1 complexes bound to the receptor for uPA, uPAR, from the cell surface, leading to lysosomal degradation of uPA and PAI-1 (for a review, see ref *9*).

In humans, a high plasma PAI-1 level is a risk factor for cardiovascular diseases (for reviews, see refs (*10*−*12*)). Evidence of a direct causal role of PAI-1 in thrombotic events comes from the observation that transgenic mice with an increased plasma PAI-1 level develop venous and arterial occlusions (*13*, *14*). uPA-catalyzed plasmin generation and the ensuing plasmin-catalyzed degradation of basement membranes are believed to enable the spread of cancerous diseases (for a review, see ref *7*). This idea is supported by evidence from model systems and the observation that high tumor levels of uPA are correlated with a poor prognosis in several cancer types (for a review, see ref *15*). Surprisingly, a high tumor level of PAI-1 is an even better marker for a poor prognosis than uPA (*16*, *17*). The tumor biological functions of PAI-1 are most likely related to a delicate balance between uPA and PAI-1 being needed to form a tumor stroma optimal for cancer cell invasion (for reviews, see refs *9* and *18*). PAI-1 is therefore a potential target for antithrombotic and anticancer therapy.

To unravel the biochemical mechanisms and physiological and pathophysiological functions of the different molecular interactions of PAI-1, specific conformational probes and inhibitors of each individual interaction are needed. We have now screened an RNA oligonucleotide library with human PAI-1 as bait. Nucleic acid aptamers are generated using the in vitro selection process termed Systematic Evolution of Ligands by Exponential Enrichment (SELEX), and this process takes advantage of the ability of short DNA or RNA oligonucleotides to fold into sequence-dependent three-dimensional structures that can recognize a great variety of targets, ranging from small molecules like metal ions, antibiotics, and organic dyes to entire cells, bacteria, and virus particles (*19*, *20*). A number of aptamers have been developed to target proteins with affinities and specificities comparable to those of antibodies. Aptamers have some additional interesting features such as low immunogenicity and small size (typically M_w values of 10000−30000) and can be generated using SELEX-compatible modified nucleoside analogues (2′-fluoropyrimidines) to increase their resistance to nucleases. We isolated PAI-1 binding aptamers that can interfere with specific biochemical functions of PAI-1 and have properties not seen with other PAI-1 binding reagents.

EXPERIMENTAL PROCEDURES

PAI-1. Human PAI-1, extended at the N terminus with a His_6 tag and a recognition motif for heart muscle kinase, was expressed in *Escherichia coli* and purified by nickel affinity chromatography and size exclusion chromatography (*21*). The purified PAI-1 was more than 95% pure, as evaluated by SDS−PAGE and Coomassie Blue staining. N-Terminal sequencing showed the expected N-terminus, i.e., MGSHHHHHHGSRRASVHH... The N-terminal extension did not affect the specific inhibitory activity of PAI-1, its second-order rate constant for reaction with uPA, its VN binding, or its rate of latency transition (*21*). The specific inhibitory activity of wild type (wt) PAI-1 was around 80% of the theoretical maximum.

Glycosylated human PAI-1 was purified from serum-free conditioned medium of dexamethasone-treated HT-1080 cells or from HEK293T cells transfected with PAI-1 cDNA by immunoaffinity chromatography (*22*, *23*). The purified latent PAI-1 was converted to the active state by denaturation with guanidinium chloride and refolding by dialysis against phosphate-buffered saline (PBS) [10 mM sodium phosphate (pH 7.4) and 140 mM

NaCl] (*22*). The remaining inactive PAI-1 was removed by affinity chromatography on immobilized β-anhydrotrypsin (*24*). Latent PAI-1 was prepared by incubation of PAI-1, at a concentration of 0.5 μM, at 37 °C for 24 h. Complete conversion to the latent state was verified by the absence of formation of a detectable complex after incubation with a molar excess of uPA, as analyzed by SDS−PAGE. The PAI-1 amino acid numbering is used throughout this paper (S1-A2-V3-H4-H5...) (*25*).

PAI-1 mutants were produced by site-directed mutagenesis with the QuickChange site-directed mutagenesis kit (Stratagene) and expressed in *E. coli*. All the tested PAI-1 mutants folded into the active conformation (*21*, *26*).

Labeling of P9-Cys in PAI-1 S340C with *N*-{[2-(iodoacetoxy)-ethyl]-*N*-methyl}amino-7-nitrobenz-2-oxa-1,3-diazole (IANBD ester, Molecular Probes), creating the fluorescent molecule PAI-$1_{P9\text{-}NBD}$, was conducted essentially as described previously (*24*). The labeling efficiency was 0.8−1.0 mol of probe/mol of PAI-1. Incorporation of the fluorescent probes at this position on PAI-1 was shown previously to have no adverse effects on PAI-1 activity (*24*, *27*). Latent PAI-1, generated during the labeling reaction, was removed by affinity chromatography on immobilized β-anhydrotrypsin (*24*).

uPA. Human uPA was purchased from Wakamoto Pharmaceutical Co. (Tokyo, Japan). The amino-terminal fragment of uPA (ATF, amino acids S1−K135) and ^{125}I-labeled uPA−PAI-1 complex were prepared as described previously (*28*, *29*).

RNA Library Construction and Aptamer Selection. Selection of aptamers to PAI-1 basically followed the guidelines described in ref *30* with minor modifications. The following oligonucleotides were obtained from DNA Technology A/S: The "Forward N35" library primer (5′-CGCGGATCCTAATACGACTCACTATAGGGGCCACCAACGACATT-3′) contains a T7 promoter sequence, and the "N35 library" primer [5′-GATCCATGGGCACTATTTATA-TCAAC(N_{35})AATGTCGTTGGTGGCCC-3′] includes the degenerate sequence. Primers were annealed and extended by Klenow enzyme [3′ → 5′ exo$^-$ (New England Biolabs)] and double-stranded DNA products purified on a 6% nondenaturing polyacrylamide gel (National Diagnostics).

The RNA library was then produced by transcription of an amount of double-stranded DNA corresponding to 10^{15} molecules in a reaction mixture with the following composition: 80 mM HEPES (pH 7.5), 30 mM DTT, 25 mM $MgCl_2$, 2 mM spermidine-HCl, 2.5 mM ATP, and 2.5 mM GTP (GE Healthcare/Amersham Biosciences), 2′-fluoro-dCTP and 2′-fluoro-dUTP (TriLink Biotechnologies), 100 μg/mL BSA (New England Biolabs), and 45 μg/mL double-stranded DNA template and 150 μg/mL mutant T7 RNA polymerase Y639F, followed by Nap-5 column (GE Healthcare/Amersham Biosciences) purification. Individual RNA aptamers was produced by a similar method but purified with an 8% denaturing polyacrylamide gel. *E. coli* BL21 cells expressing T7 RNA polymerase mutant Y639F were a kind gift from R. Sousa (University of Texas Health Science Center, San Antonio, TX). In contrast to wt T7 polymerase, this mutant efficiently utilizes 2′-fluoropyrimidines as a substrate. The mutant polymerase was expressed and purified as described previously (*31*, *32*). RNA sequences with affinity for PAI-1 were selected using PAI-1-conjugated Sepharose. Ten milligrams of Protein A Sepharose (GE Healthcare/Amersham Biosciences) was incubated overnight with 10 μg of a rabbit polyclonal anti-PAI-1 antibody in HEPES-buffered saline (HBS) [30 mM HEPES (pH 7.4) and 135 mM NaCl] supplemented with 0.01% Tween 20 overnight at 4 °C, followed by washing. One half of the antibody-conjugated beads were used for counter selection to remove RNA sequences binding to the Protein A Sepharose or the antibodies. The other half was incubated with 5 μg of PAI-1 from HT-1080 cells for 30 min at room temperature, followed by washing. In the first selection round, counter selection beads were incubated with 5×10^{15} RNA oligonucleotides in HBS (pH 7.2) containing 2 mM $MgCl_2$, 25 μg/mL tRNA (Sigma-Aldrich), 25 μg/mL poly-AGC (Sigma-Aldrich), and 100 μg/mL BSA (New England Biolabs) for 30 min at room temperature. Unbound material was then passed onto PAI-1-conjugated beads for 30 min at room temperature. After being extensively washed, bound RNA sequences were eluted by proteinase K digestion (New England Biolabs). Library RNA sequences were annealed to reverse transcription primer "Reverse N35" (5′-CCCGACACCCGCGGATCCATG-GGCACTATTTATATCAA-3′) and reverse transcribed using AMV RT (Promega). Double-stranded DNA transcription templates for the next round of selection were then generated by PCR (Taq system, Invitrogen) using Forward N35 and Reverse N35 primers, followed by BamHI digestion (New England Biolabs). RNA for subsequent rounds of selection was produced in the presence of trace amounts of [α-^{32}P]dATP and purified by Nap-5 columns (rounds 2−5) or on a 12% denaturing polyacrylamide gel (rounds 6−8). In rounds 2−5, 500 nM RNA was applied in the selection procedure, while the amount was 100 nM in rounds 6−8. Scintillation counting was applied to follow the amount of RNA retained by PAI-1-conjugated Sepharose beads for every selection round.

To identify individual PAI-1 binding RNA sequences, the pool of double-stranded DNA transcription templates after round 8 was ligated into plasmid vectors according to the manufacturer's protocol (TOPO TA Cloning Kit, Invitrogen).

Aptamer Extinction Coefficient and Secondary Structure Prediction. The aptamer molar extinction coefficient and precise molecular mass were calculated using the online calculator tool Oligocalc (http://www.basic.northwestern.edu/biotools/oligocalc.html). The secondary structure of the selected aptamers was predicted with the web-based program mfold. The prediction is based on minimum free energy calculations (*33*, *34*).

Aptamer−PAI-1 Surface Plasmon Resonance Binding Assays. Surface plasmon resonance (SPR) analysis was performed on a BIACORE T100 instrument at 25 °C. Active, latent, or reactive center-cleaved PAI-1 wt or PAI-1 mutants were captured on monoclonal anti-PAI-1 antibody mAb-1 (*35*) immobilized on a CM5 sensor chip. mAb-1 immobilization was performed by amine coupling to a level of approximately 2000 response units (RU). All binding reactions were performed in a buffer of HBS (pH 7.4) supplemented with 2 mM $MgCl_2$ and 0.05% Tween 20. PAI-1 was captured via injection of a 40 nM PAI-1 solution at a flow rate of 30 μL/min, reaching capture levels of 300−500 RU. Concentration series of the aptamers (0.5−30 nM) were injected at a flow rate of 20 μL/min. The sensor chip surface was regenerated with 10 mM glycine (pH 2.5) and 1 M NaCl after each run. Binding of <5 RU to a captured PAI-1 mutant was considered as no binding.

The uPA−PAI-1 complex was captured on soluble urokinase-type plasminogen activator receptor (uPAR; a kind gift from M. Ploug, Finsen laboratory), immobilized on a CM5 sensor chip to a level of 2000 RU. uPA was captured on the immobilized uPAR by injection of a 100 nM uPA solution. Following the capture of uPA, 100 nM *E. coli* PAI-1 or 200 nM HT1080 PAI-1 was injected, leading to the formation of the uPA−PAI-1 complex

on the immobilized uPAR. The aptamers were then introduced at concentrations between 0.50 and 130 nM. Regeneration was achieved with 0.1 M acetic acid and 0.5 M NaCl.

All binding reactions were analyzed by the kinetic software in the BIACORE T100 evaluation program and K_D values estimated from association and dissociation rates based on a 1:1 stoichiometry.

PAI-1−Vitronectin Surface Plasmon Resonance Binding Assays. Monomeric vitronectin was immobilized on a BIACORE CM5 sensor chip to a level of 500 RU. The binding of 5 nM wt PAI-1, PAI-1 K124A, or PAI-1 R78A to the vitronectin-coated chip was assessed in the presence of the aptamer at concentrations between 0 and 15 nM.

Fluorescence Spectroscopy. Fluorescence measurements were taken on a PTI Quantamaster instrument, equipped with rapid Peltier temperature-controlled single-sample holder. All experiments were performed in quartz cuvettes using a 1500 μL sample in 20 mM Tris-HCl (pH 7.4), 150 mM NaCl, and 2 mM $MgCl_2$, supplemented with 0.1% (w/v) PEG6-8000 and at a temperature kept constant at 22 °C. Fluorescence emission spectra were recorded from 304 to 450 nm in 2 nm steps, with an excitation wavelength of 295 nm. All spectra were recorded using a PAI-1 or aptamer concentration of 50 nM, and all spectra were corrected with a buffer spectrum. Reactive center-cleaved 14-1B PAI-1, as used in the experiments, was prepared according to the method described in ref *6*.

Binding experiments were performed with a fixed paionap-5 concentration of 40 nM while the PAI-1 concentration was increased by addition of a series of 2 μL aliquots of a PAI-1 stock solution, reaching a final PAI-1 concentration between 60 and 70 nM after additions of up to 40−50 μL. The fluorescence change was measured at the wavelength of maximum perturbation, outside the Raman water peak (318−335 nm) at 340 nm. Each point was an average of a 90 s recording. The titration curve was corrected for added fluorophore by subtraction of a corresponding titration curve of PAI-1 into buffer. The resulting curve was fitted to a 1:1 binding isotherm with floating F_{max}, K_D, N, and P_0 values.

$$F = \frac{F_{max}[NP_0 + K_D + L_0 - \sqrt{(NP_0 + K_D + L_0)^2 - 4NP_0L_0}]}{2NP_0} \quad (1)$$

where F is a function of the titrant concentration (L_0), P_0 is the aptamer concentration in the cuvette, K_D is the dissociation constant, F_{max} equals F at saturation where $L_0 \gg P_0$ ($N = 1$), and N is the stoichiometry of the reaction.

Radioactive Labeling of RNA. In vitro-transcribed RNA was dephosphorylated using calf intestinal phosphatase (New England Biolabs) and subsequently extracted with a phenol/chloroform mixture and 5′ end-labeled using T4 polynucleotide kinase (New England Biolabs). End-labeled RNA was diluted to approximately 0.1 μM following gel purification and a second round of phenol/chloroform extraction. Size markers were the 5′-end-labeled 25 bp DNA ladder (Invitrogen) and Decade Marker (Ambion). We prepared the T1 sequencing ladder by mixing 5′-end-labeled RNA and tRNA carrier in 20 μL of G buffer [20 mM sodium citrate (pH 5.0), 1 mM EDTA, and 7 M urea] and incubating the mixture for 5 min at 50 °C prior to the addition of 1 μL of T1 (50 units/mL, Ambion) and further incubation for 15 min at 50 °C.

Electrophoretic Mobility Shift Assay (*EMSA*). Binding reactions were performed by incubation of 5′-end-labeled RNA with PAI-1 in binding buffer [30 mM HEPES (pH 7.4), 135 mM NaCl, and 2 mM $MgCl_2$] followed by incubation for 15 min at room temperature. The mixtures were analyzed for complex formation on a 6% native polyacrylamide gels and visualization using a phosphorimager (Bio-Rad).

RNA Modification Using Ethylnitrosourea (*ENU*). In vitro-transcribed 5′-end-labeled RNA was modified according to the protocol described in ref *36*. Ten microliters of H_2O and RNA (50 ng/106 cpm) was mixed with 10 μL of 2× modification buffer [600 mM sodium cacodylate (pH 8.0) and 10 mM EDTA] and 5 μL of saturated ENU (750 mM) and incubated for 2 min at 80 °C, followed by precipitation and resuspension in binding buffer [30 mM HEPES (pH 7.4), 135 mM NaCl, and 2 mM $MgCl_2$]. After selection and purification on a native PAGE gel, modification-specific backbone cleavage was induced by resuspension of the RNA in 10 μL of strand scission buffer [100 mM triethylammonium bicarbonate (pH 9.0)] and incubation at 50 °C for 5 min. The resulting cleavage products were resolved on a 15% denaturing polyacrylamide gel.

RNase Footprinting of RNA−Protein Complexes. Footprinting studies were performed with the binding conditions described above for RNA−protein complexes. Enzymes T2 (Sigma) and V1 (Ambion) were added in concentrations of 0.5 U/mL and 10 U/mL respectively, and samples were incubated for 2 min at room temperature followed by addition of urea loading buffer and analysis on a 15% denaturing polyacrylamide gel. All mapping experiments were controlled for the expected formation of RNA−protein complexes by an EMSA (data not shown).

Determination of PAI-1 Specific Inhibitory Activity. To measure the specific inhibitory activity of PAI-1, i.e., the fraction of PAI-1 capable of inhibiting the proteolytic activity of uPA, aliquots of PAI-1 were serially diluted in HBS supplemented with 0.25% gelatin and 2 mM $MgCl_2$, giving PAI-1 concentrations between 0.5 ng/mL (11 pM) and 0.5 μg/mL (11 nM). One volume of 0.05 μg/mL uPA in HBS with gelatin was added to each well, followed by incubation for at least 5 min. The remaining uPA activity was determined via addition of the chromogenic substrate S-2444 [pyro-Glu-Gly-Arg-*p*-nitroanilide (Chromogenix)] to a final concentration of 70 μM and measurement of the absorbance at 405 nm after 30 min. The specific inhibitory activity of PAI-1 was calculated from the amount of PAI-1 that inhibited 50% of the uPA. When the effect of the aptamers was assayed, these were added to all wells of a dilution series using a constant saturating concentration.

Protection of PAI-1 from Inactivation by bis-ANS. The specific inhibitory activity of PAI-1 was determined, as described above, in the absence or presence of bis-ANS. Dilution series of PAI-1 were incubated either in buffer, in the presence of aptamers, or in the presence of vitronectin. Then, 0.5 μM bis-ANS was added, followed by incubation for 10 min before the addition of uPA.

Latency Transition Assays. PAI-1 (0.5 μg/mL) was incubated at 37 °C in a buffer of HBS supplemented with 0.25% gelatin and 2 mM $MgCl_2$, in the absence and presence of paionap-5, paionap-40, or control RNA aptamers (0.3 μg/mL). After different time periods, the specific inhibitory activity of PAI-1 was measured. The half-life for latency transition was calculated from semilogarithmic plots of the specific inhibitory activity versus time.

Insertion Peptide Inactivation Assays. The peptide used was TVASS, acetylated at the N-terminus and amidated at the

C-terminus. PAI-1 (0.5 μg/mL) was incubated at 37 °C in HBS buffer with 0.25% gelatin, in the absence or presence of aptamers (0.3 μg/mL) and in the absence or presence of TVASS (125 μM). After different incubation periods, the remaining specific inhibitory activity of PAI-1 was measured. The half-life for inactivation was calculated from semilogarithmic plots of the specific inhibitory activity versus time.

Determination of Second-Order Rate Constants for uPA−PAI-1 Binding. The apparent second-order rate constant for the irreversible inhibition of uPA by PAI-1 in the absence and presence of aptamers (65 nM) was determined by a competitive kinetic method with the chromogenic substrate S-2444. Reactions were performed under pseudo-first-order conditions, in which PAI-1 (1.25−50 nM) was at a minimum level in a 5-fold molar excess of uPA (0.25 nM). The reactions were performed in the presence of S-2444 (3 mM), and the progression curve was monitored at 405 nm every minute for 60 min. The progression curve (A_{405} vs time) was fitted to a single-exponential function, and k_{obs} values for each PAI-1 concentration were estimated on the basis of eq 2 (*37*).

$$[P]_t = [P]_0 + [P]_\infty(1 - e^{-k_{obs}t}) \quad (2)$$

where $[P]_t$, $[P]_0$, and $[P]_\infty$ are the product concentrations at time t, time zero, and time infinite, respectively, proportional to the recorded A_{405} values. The observed k_{obs} values were plotted versus PAI-1 concentrations. K_m and k_{lim} were determined by fitting the data to eq 3.

$$k_{obs} = k_{lim}[PAI\text{-}1]_0/[K_D(1 + [S\text{-}2444]/K_m) + [PAI\text{-}1]_0] \quad (3)$$

where [S-2444] is the concentration of S-2444 at time zero and $[PAI\text{-}1]_0$ the PAI-1 concentration at time zero. The K_m for S-2444 is 0.1 mM. The second-order rate constant k_2 is given by k_{lim}/K_D.

Stopped-Flow Fast Kinetic Analysis. The reactions of PAI-$1_{P9\text{-}NBD}$ (10 nM) with uPA (0.05−4 μM) in the absence or presence of aptamer (16 nM) were assessed on an Applied Photophysics SX.18MV stopped-flow reaction analyzer with a thermostated syringe chamber. All samples were diluted in SF buffer [30 mM HEPES (pH 7.4), 135 mM NaCl, 2 mM $MgCl_2$, and 0.1% PEG 8000]. PAI-$1_{P9\text{-}NBD}$ and aptamers were preincubated for 10 min at room temperature before the reactions. Excitation was at 480 nm, and fluorescence emission was measured with a cutoff below 515 nm and a 9.3 nm band-pass. For each uPA concentration, four to nine reactions with PAI-$1_{P9\text{-}NBD}$ alone or in complex with the aptamer were measured. The k_{obs} value for each reaction was determined by fitting the data to a single-exponential function. An average was calculated for each uPA concentration. The k_{obs} values were plotted versus the uPA concentration. The k_{lim} and K_m values were determined by a nonlinear regression analysis of the plots of k_{obs} versus the uPA concentration according to eq 4:

$$k_{obs} = \frac{k_{lim}[uPA]_0}{K_m + [uPA]_0} \quad (4)$$

Solid Phase Receptor Binding Assays. VLDLR and LRP were coated onto 96-well Maxisorp microtiter wells overnight at 4 °C in 50 mM $NaHCO_3$ (pH 9.6) at a concentration of 1 μg/mL. The wells were blocked with 10% BSA in binding buffer [10 mM HEPES (pH 7.8), 140 mM NaCl, 2 mM $CaCl_2$, and 1 mM $MgCl_2$] for 2 h, washed, and incubated overnight at 4 °C with 20 pM [^{125}I]uPA−PAI-1 complex. Washing and incubation with ligands were performed in binding buffer with 1% BSA. When the effect of aptamers on binding of the [^{125}I]uPA−PAI-1 complex to receptors was investigated, aptamers were added at concentrations from 1 to 130 nM. Aptamers were preincubated with the complex for 15 min prior to the incubation with the solid phase bound receptor. After the incubation, the supernatants were removed for γ-counting and the wells washed. Bound ligand was solubilized with 10% SDS and taken for γ-counting. The concentration of bound ligand was corrected for nonspecific binding, i.e., the radioactivity recovered from wells without receptor, and plotted versus the total aptamer concentration. The K_D value (K_{D2}) for the binding of the aptamers to the uPA−PAI-1 complex was determined by fitting the data to eq 5.

$$\text{bound} = \frac{a}{2} - \sqrt{\frac{a^2}{4} - [^{125}\text{I-uPA}-\text{PAI-1}]_{total}[\text{receptor}]_{total}} \quad (5)$$

where $a = [^{125}\text{I-uPA}-\text{PAI-1}]_{total} + K_{D1} + [\text{receptor}]_{total} + (K_{D1}/K_{D2})[\text{aptamer}]_{total}$ and K_{D1} symbolizes the K_D value for binding of the uPA−PAI-1 complex to LRP [0.4 nM (*7*)] or VLDLR [1.5 nM (*38*)].

Receptor-Mediated Ligand Degradation Assays. U937 cells (American Type Culture Collection, CR1 1593) were cultured in RPMI medium with 10% fetal calf serum (*39*). For analysis of receptor-mediated ligand degradation, the cells were incubated in serum-free medium supplemented with 0.5% BSA at a density of 10×10^6 cells/mL, with 10 pM [^{125}I]uPA−PAI-1 complex and aptamers, receptor-associated protein, and/or ATF, at concentrations as described for each individual experiment. After incubation for 2 h at 37 °C, we determined the fraction of complex that had been degraded by making the cultures 7% with respect to trichloroacetic acid and centrifuging them. The radioactivity in pellets and supernatants was determined, and the fraction of degraded ligand was scored as the fraction of radioactivity soluble in 7% trichloroacetic acid (*40*).

RESULTS

Selection of Aptamers. A library of RNA oligonucleotides containing a random region of 35 nucleotides, prepared with 2′-fluoropyrimidines, was screened with glycosylated PAI-1 in the active form as bait. From round 6 to 8 in the selection, we observed a significant increase in the amount of ^{32}P-labeled RNA retained on the PAI-1-conjugated beads after selection and therefore identified the sequences of individual clones after round 8. Two sequences were selected for further analysis. The corresponding aptamers will be termed paionap-5 and paionap-40 (Table 1).

Binding of Aptamers to PAI-1. We next analyzed the binding of paionap-5 and paionap-40 to different forms of PAI-1 by the use of SPR. A monoclonal anti-PAI-1 antibody was immobilized and used to capture PAI-1 in different conformations. The antibody used for immobilization, mAb-1, binds an epitope in α-helix C (*35*) and was chosen because we expected the aptamers to bind the relatively basic α-helix D, distant from α-helix C. To analyze binding of the aptamer to the uPA−PAI-1 complex, we captured the complex on a chip coated with urokinase-type plasminogen activator receptor (uPAR), which binds uPA by its N-terminal growth factor domain. In this setup, only PAI-1 that is in complex with uPA is presented on the chip, thereby avoiding misleading results from noncomplexed PAI-1. The binding of the aptamers to the captured PAI-1 was then measured by application of different concentrations of the aptamers to the

Table 1: Sequences of the Selected RNA Aptamers[a]

aptamer	sequence
paionap-5	GGGGCCACCAACGACAUU**GAACCACGUAGGCUCGUUUCUGAGCCGAUCUCGAU**GUUGAUAUAAAUAGUGCCCAUGGAUC
paionap-40	GGGGCCACCAACGACAUU**UAUCGAAUUGAUAACCUUACGCGAGAGCGUAGUUC**GUUGAUAUAAAUAGUGCCCAUGGAUC

[a]The variable regions are highlighted in bold.

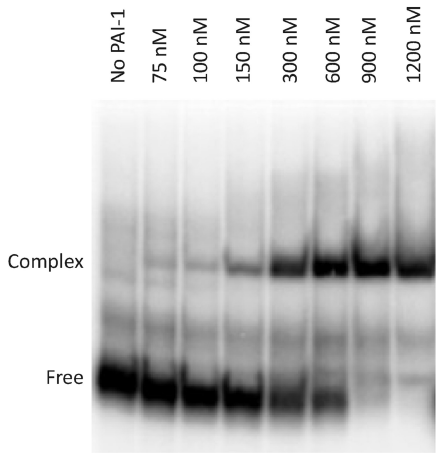

FIGURE 2: EMSA of [^{32}P]paionap-5 binding to PAI-1. Approximately 300 nM ^{32}P-end-labeled paionap-5 was incubated with the indicated concentrations of *E. coli*-expressed PAI-1 in the active conformation for 15 min at room temperature. The incubation mixtures were then subjected to nondenaturing polyacrylamide gel electrophoresis. The radioactive bands were visualized with autoradiography. Labels indicating the migration of the free and PAI-1-complexed aptamer are shown at the left.

chip. By these analyses, we found PAI-1−aptamer binding kinetics to be compatible with a simple 1:1 binding model. A simple 1:1 binding model was supported by EMSA analysis of formation of the aptamer−PAI-1 complex, exemplified with paionap-5 (Figure 2). At molar ratios at which either PAI-1 or aptamer was in excess, only one slower migrating aptamer−PAI-1 complex band was formed. In our SPR analyses, we found that paionap-5 bound glycosylated as well as nonglycosylated PAI-1 in the active, latent, reactive center-cleaved, or protease-complexed form, with K_D values in the low nanomolar range (Table 2). Glycosylated PAI-1 bound with a slightly lower affinity than nonglycosylated PAI-1, particularly in the loop-inserted forms. In contrast, paionap-40 bound measurably only to the active form, not the RCL-inserted forms (Table 2). The K_D of the interaction of paionap-40 with RCL-inserted forms was in each case estimated to be at least 10 times higher than the highest tested concentration at which no binding was observed. We observed no binding to murine PAI-1 (data not shown).

An independent determination of the PAI-1−aptamer binding affinity was done by measurement of tryptophan fluorescence in the absence and presence of aptamers. The fact that PAI-1 contains four tryptophan residues, with at least two in the vicinity of the presumed aptamer binding surface, suggested that perturbation of intrinsic tryptophan fluorescence could be used as a tool to study PAI-1−aptamer binding. A reactive center-cleaved version of the stable variant 14-1B PAI-1 (*41*) was used to avoid interpretation ambiguities due to latency transition during the assay, the lower solubility of the other forms, or the presence of latent PAI-1 in the cleaved samples. paionap-5 was chosen on the basis of its ability to bind both stressed and relaxed conformations of PAI-1. The addition of the aptamer resulted in a clear increase in the tryptophan fluorescence compatible with a markedly changed environment of at least one tryptophan in PAI-1 (Figure 3). paionap-5 did not by itself exhibit any appreciable fluorescence. The binding affinity of PAI-1 for paionap-5 was estimated at the 340 nm emission wavelength. Addition of increasing amounts of the reactive center-cleaved PAI-1 resulted in a saturable binding curve. The binding curves could be fitted to a 1:1 binding model, and a K_D of 1.9 ± 0.6 nM was in agreement with the tight binding observed by SPR.

Mapping of the Binding Site for Aptamers on PAI-1 by Site-Directed Mutagenesis. We next mapped the binding site for the aptamers on PAI-1 by the use of site-directed mutagenesis. The aptamer binding to various PAI-1 mutants was analyzed by SPR, using preparations of nonglycosylated PAI-1 in the active conformation. In most cases, Ala substitutions were used. All mutant preparations used in the SPR experiments contained approximately the same high fraction of active PAI-1 as the wt. By this analysis, a group of residues at the top of α-helix E and the bottom of α-helix D was found to be essential for paionap-5 binding. The same group of residues was shown to be essential also for paionap-40 binding. In the special case of Lys124, binding kinetics similar to those of wt were observed for paionap-5 [$k_{on} = 2.6 \pm 1.2\ \mu M^{-1}\ s^{-1}$, $k_{off} = 0.0023 \pm 0.0006\ s^{-1}$, and K_D = 1.1 ± 0.5 nM (n = 5)], whereas no binding to paionap-40 was detected with concentration of up to 65 nM. The binding sites for the two aptamers overlap with, but are clearly distinct from, the binding site for vitronectin. For instance, the triple mutant R103A/M112A/Q125A is without detectable binding to vitronectin (*42*) but binds normally to the aptamers (Figure 1).

Mapping of the Binding Site for PAI-1 on Aptamers. To characterize the aptamer regions directly involved in PAI-1 binding, we used RNase footprinting and phosphate modification interference analyses. For the RNase footprinting analysis, we used the double-strand-specific RNase V1 and the single-strand-specific RNase T2. The phosphate modification interference technique involves ethylation of backbone phosphates by ENU treatment, thereby allowing assessment of binding of PAI-1 to phosphate at specific positions in the RNA. After selection of modified RNA in fractions bound or unbound by PAI-1, backbone cleavage was induced at ethylated phosphates by mild alkaline treatment. This resulted in a cleavage pattern in which the absence of signal revealed positions where phosphate ethylation prevented the RNA aptamer from binding PAI-1. Formation of RNA−protein complexes was confirmed by EMSAs in all cases. With RNase footprinting as well as phosphate modification interference, the use of 2′-fluoropyrimidines in the aptamers limited the analysis to purines.

With paionap-5, the phosphate modification interference analysis showed a clear difference in signal intensity for bound and unbound RNA in positions 24−29 and 41 and 42 (marked by bars in Figure 4A), indicating that these backbone phosphates serve as critical binding sites for PAI-1. No cleavage was seen for control RNA not treated with ENU (Figure 4A, left panel), confirming the specificity of the mapping. The RNase footprinting

Table 2: Binding of Different Forms of PAI-1 to Aptamers[a]

	paionap-5			paionap-40		
PAI-1 variant	k_{on} (μM^{-1} s^{-1})	k_{off} (s^{-1})	K_D (nM)	k_{on} (μM^{-1} s^{-1})	k_{off} (s^{-1})	K_D (nM)
E. coli active	1.78 ± 0.29 (3)	0.0028 ± 0.0008 (3)	1.58 ± 0.34 (3)	4.15 ± 0.79 (3)	0.0050 ± 0.0016 (3)	1.23 ± 0.43 (3)
E. coli latent	0.664 ± 0.078 (3)	0.0017 ± 0.0001 (3)	2.56 ± 0.12 (3)	no measurable binding at 65 nM[c]		
E. coli complex	0.866 ± 0.361 (3)	0.0026 ± 0.0007 (3)	3.18 ± 1.04 (3)	no measurable binding at 130 nM[c]		
14-1B active	1.12 ± 0.25 (3)	0.0038 ± 0.0001 (3)	3.52 ± 0.80 (3)	2.01 ± 0.62 (3)	0.0045 ± 0.0013 (3)	2.27 ± 0.10 (3)
14-1B cleaved	0.628 ± 0.099 (3)	0.0024 ± 0.0005 (3)	3.72 ± 0.31 (3)	no measurable binding at 65 nM[c]		
HT-1080 active	0.555 ± 0.053 (3)	0.0021 ± 0.0009 (3)	3.77 ± 1.26 (3)	2.63 ± 0.11 (3)	0.0097 ± 0.0043 (3)	3.66 ± 1.54 (3)
HT-1080 latent	0.471 ± 0.119 (3)	0.0072 ± 0.0002 (3)	16.2 ± 6.17 (3)[b]	no measurable binding at 65 nM[c]		
HT-1080 complex	0.504 ± 0.198 (3)	0.0049 ± 0.0021 (3)	9.71 ± 0.39 (3)[b]	no measurable binding at 65 nM[c]		

[a]A BIACORE chip was coated with monoclonal anti-PAI-1 mAb-1 (for analysis of active, latent, or reactive center-cleaved PAI-1) or uPAR (for analysis of the uPA−PAI-1 complex) to a density of approximately 2000 RU/mm^2. Between 100 and 500 RU of the indicated form of PAI-1 was captured on the chip. For cleaved PAI-1, we used a trypsin-treated form of the PAI-1 variant 14-1B expressed in *E. coli*, which could be produced without significant contamination with latent PAI-1 (*21*). Different concentrations of paionap-5 or paionap-40 were applied, and the k_{on}, k_{off}, and K_D values were calculated from the time course of association and dissociation using the BIACORE T100 evaluation software. Means, standard deviations, and numbers of determinations are given. [b]Significantly different from the K_D for active HT-1080 PAI-1 ($p < 0.01$) and significantly different from the K_D values for the corresponding forms of *E. coli* ($p < 0.01$). [c]The K_D values were estimated to be at least 10 times higher than the highest tested concentration at which no binding was observed.

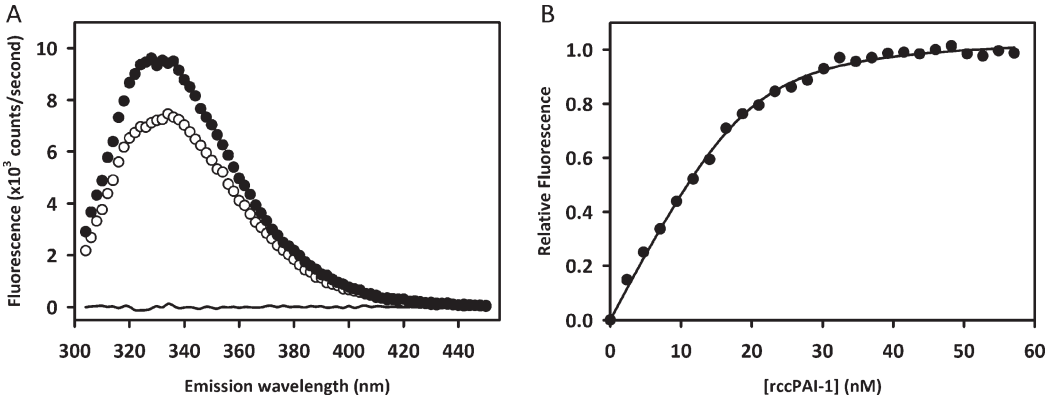

FIGURE 3: Intrinsic tryptophan fluorescence used to study the binding of PAI-1 to paionap-5. (A) Emission spectra of reactive center-cleaved PAI-1 (○), 50 nM paionap-5 (—), and the mixture (●). (B) Change in tryptophan fluorescence at 340 nm for 26 nM paionap-5 and the indicated concentrations of reactive center-cleaved PAI-1. Values were corrected for reactive center-cleaved PAI-1 fluorescence, normalized, and averaged for three independent titrations, with a best fit to a 1:1 binding model. rccPAI-1 stands for the reactive center-cleaved PAI-1.

analysis supported these findings by showing a PAI-1-induced protection from RNase V1 in positions 20−30 as well as positions 41 and 42 (Figure 4B). The protection pattern observed with RNase T2 supports the fact that the flexible loop in positions 20−30 of the aptamer is involved in binding; moreover, an altered processing in the constant region upon addition of PAI-1 (position 55 for V1 and position 62 for T2) suggests that protein binding could alter the RNA structure flanking the binding site (Figure 4C). As expected from the mutagenesis analysis, no protection was observed with the double mutant PAI-1 R117E/R120E (data not shown). The interactions between paionap-5 and PAI-1, as mapped by ENU and RNase treatment, are summarized on the predicted aptamer secondary structure in Figure 4D.

A similar interaction analysis was conducted for the paionap-40−PAI-1 complex (data not shown). The phosphate modification interference analysis showed positions 16, 31−37, and 54 to be sensitive to ENU modification. The region of paionap-40 protected from RNase V1 degradation largely coincided with the areas sensitive to ENU treatment, although RNase V1 footprinting extended beyond the region sensitive to ENU modification, suggesting a region with a lower binding affinity or interactions independent of backbone phosphates. No protection was observed when the paionap-40−PAI-1 complex was digested with RNase T2, due to the predominance of 2′-fluoropyrimidines in single-stranded parts of the PAI-1 binding region of paionap-40. Thus, the PAI-1 binding site on paionap-40 appears to be a central bulge in which two small stems divide (Figure 4E). The overall binding surface on the RNA aptamer is larger for paionap-40 than for paionap-5, in agreement with the finding from site-directed mutagenesis of PAI-1 described above.

Effects of Aptamers on PAI-1−Vitronectin Binding. Since the binding sites on PAI-1 for the aptamers and vitronectin overlap, we looked for possible effects of the aptamers on the interaction between PAI-1 and vitronectin. Vitronectin was immobilized on a BIACORE chip. When PAI-1 was applied, high-affinity binding was observed (*43*). Upon addition of PAI-1, which had been preincubated with either of the two aptamers, the binding was strongly inhibited, with an IC_{50} in the low nanomolar range, in good agreement with the K_D determinations described above (Figure 5). The interaction between vitronectin and PAI-1 mutant R78A, which retains normal vitronectin affinity but is incapable of aptamer binding, was not inhibited by the aptamers. Interestingly, vitronectin binding of mutant K124A was strongly inhibited by paionap-5, which has an affinity similar to that of the mutant for wt PAI-1, but only slightly affected by paionap-40, which displays a very low affinity for this mutant.

Effects of Aptamers on the Reaction of PAI-1 with uPA. We evaluated the effect of the aptamers on the antiproteolytic

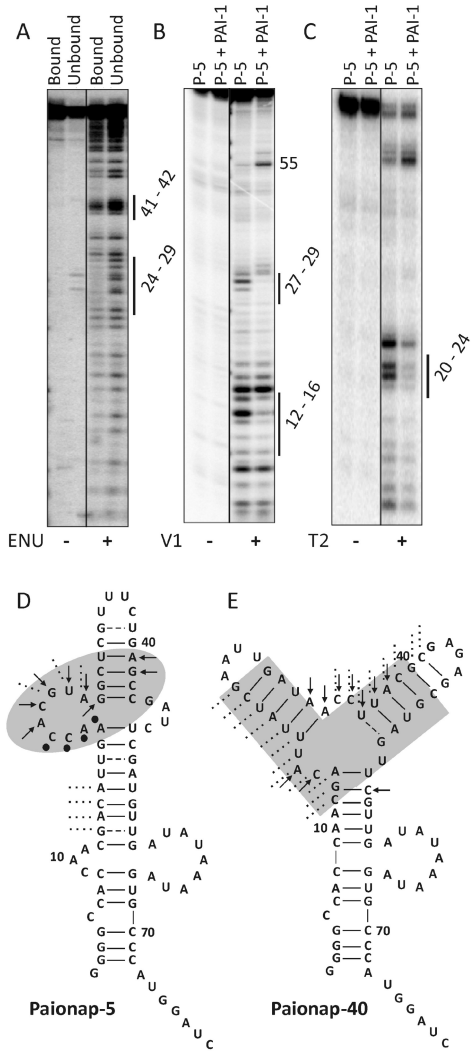

FIGURE 4: Mapping of the binding site for PAI-1 on the aptamers. (A) Phosphate modification interference. Cleavage products resulting from ENU- or control-treated paionap-5 selected by an EMSA in fractions bound or unbound by PAI-1. Black bars indicate positions where ENU-modified RNA is under-represented in the bound fraction, showing position to be important for RNA−protein interaction. (B) RNase V1 footprint of paionap-5 bound by PAI-1. Black bars indicate regions protected from degradation by the presence of PAI-1. (C) RNase T2 footprint of paionap-5 bound by PAI-1. Black bars indicate regions protected from degradation by the presence of PAI-1. (D) RNA−protein interaction sites mapped onto the secondary structure of paionap-5 as predicted by mfold (*30*, *31*). Arrows indicate positions sensitive to ENU modification; dashed lines show regions protected from V1 cleavage, while filled circles denote regions protected from T2 degradation. The overall region of RNA−protein contacts summarizing findings from mapping studies is colored gray. (E) RNA−protein interaction sites mapped onto the secondary structure of paionap-40 as predicted by mfold (*30*, *31*). All symbols are the same as for paionap-5. P-5 stands for paionap-5.

effect of PAI-1 by measuring its specific inhibitory activity toward uPA or tPA in the absence and presence of aptamers. There was no measurable effect of any of the two aptamers. We also demonstrated that the aptamers had no direct effects on the activity of the plasminogen activators (data not shown). The effect of the aptamers on the PAI-1−uPA interaction was also evaluated by measurements of second-order rate constants for the reaction between the two. The second-order rate constants for the reaction of PAI-1 with uPA without additions, with paionap-5, or with paionap-40 were determined to be $(0.82 \pm 0.32) \times 10^7$ ($n = 6$), $(3.18 \pm 1.38) \times 10^7$ ($n = 4$), and $(2.17 \pm 1.08) \times 10^7$ M^{-1} s^{-1} ($n = 4$), respectively. These values correspond to a small but significant increase ($p < 0.025$ by the Student's t test) in the second-order rate constant in the presence of both PAI-1 binding aptamers.

Furthermore, the effect of the aptamers on the reaction between PAI-1 with uPA was studied by the use of a PAI-1 variant labeled with the fluorescent tag NBD at the P9 residue. The tag becomes buried under α-helix F when the RCL is inserted into β-sheet A during complex formation or serpin substrate behavior, resulting in an increase in fluorescence emission (*44*). The fluorescence change can be followed by stopped flow-fast kinetic analysis. Determining the rate constant for RCL insertion, k_{obs}, at several uPA concentrations, a K_m, and a k_{lim} can be accomplished using eq 4. Both aptamers, paionap-40 most strongly, caused a reduction in k_{lim} as well as K_m (Figure 6 and Table 3). Since the second-order rate constant according to theory equals k_{lim}/K_m, the observed changes in k_{lim} and K_m correspond to a small increase in the second-order rate constant, in complete agreement with results obtained by direct measurement of this constant (see above).

Effects of Aptamers on Latency Transition. To investigate whether the aptamers affect the rate of conversion of PAI-1 from the active to the latent state, we measured the specific inhibitory activity of PAI-1 after various time periods during incubations at 37 °C. Without additions, the specific inhibitory activity was lost with a half-life of ~60 min. There was a striking delay in the loss of specific inhibitory activity in the presence of either of the two aptamers, most strongly with paionap-40, which caused an up to 8-fold increase (Table 4).

Effects of Aptamers on the Rate of Inactivation of PAI-1 by RCL-Mimicking Peptides. The antiproteolytic action of serpins can be inactivated by peptides with the same sequence as the N-terminal part of the RCL (*45*). The peptides insert as strand 4 into β-sheet A and prevent insertion of the RCL during reaction with target proteases, inducing serpin substrate behavior (*46*). Recently, the rate of inactivation of PAI-1 by an RCL-mimicking peptide was used to probe the "openness" of the gap between β-strand 5 and β-strand 3 (*47*). We therefore measured the rate of inactivation of PAI-1 by an excess of the peptide TVASS in the absence or presence of paionap-5 or paionap-40. With 10 nM *E. coli* PAI-1, 125 μM TVASS, and 0.3 μg/mL aptamer, the inactivation half-lives were 7.90 ± 0.46 min ($n = 4$) without aptamer, 5.57 ± 0.89 min ($n = 3$) with paionap-5, 39.7 ± 4.6 min ($n = 3$) with paionap-40, and 7.93 ± 0.00 min ($n = 3$) with a control aptamer. These values correspond to statistically significant effects of paionap-5 and paionap-40 on the inactivation rate ($p < 0.01$).

Effects of Aptamers on Inactivation of PAI-1 by Organochemical Compounds. We previously demonstrated that bis-ANS, with an IC_{50} of ~0.5 μM, causes a rapid and irreversible inactivation of the antiproteolytic activity of PAI-1, due to a rapid conversion of active PAI-1 to a form exhibiting substrate behavior, followed by conversion to inert polymers over the course of a few minutes (*48*, *49*). PAI-1 is protected against the inactivating effect of bis-ANS by vitronectin (*21*, *48*). Since the RNA aptamers described here bind in the same region as vitronectin, we tested whether the aptamers protect PAI-1 against bis-ANS inactivation. We measured the specific inhibitory activity of PAI-1 with various combinations of bis-ANS and aptamers (Figure 7). The specific inhibitory activity of PAI-1 was reduced 5-fold by the presence of 0.5 μM bis-ANS. Equimolar amounts of each

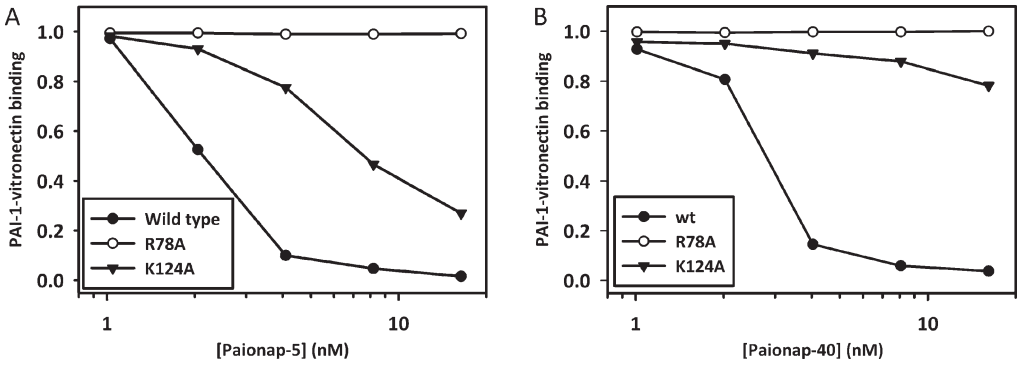

FIGURE 5: PAI-1 binding aptamers inhibit PAI-1−vitronectin binding. Vitronectin was coated on a CM5 BIACORE chip to a density of 500 RU/mm^2; 5 nM PAI-1 (wt or R78A or K124A mutant) was applied to the chip in the presence of paionap-5 (left) or paionap-40 (right) in the indicated concentrations. The binding at each combination of aptamer and PAI-1 is expressed relative to the observed response with wt PAI-1 alone.

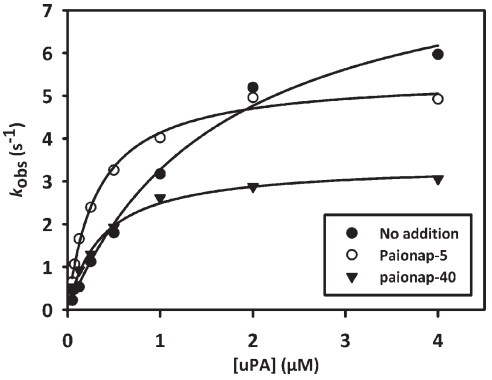

FIGURE 6: Effects of aptamers on the rate of protease inhibition by PAI-1. The reaction between 10 nM P9-NBD-PAI-1 and the indicated concentrations of uPA in the absence (●) or presence of 16 nM paionap-5 (○) or 16 nM paionap-40 (▼) was characterized by stopped-flow fast kinetic analysis. The fluorescence emission was measured at a wavelength of 527 nm, with excitation at 480 nm. Average k_{obs} values from four to nine acquisitions at each uPA concentration were plotted vs the uPA concentration. The experiment shown in the figure is a representative from three independent experiments. The K_m and k_{lim} values, determined by fitting the data to eq 4 in all three experiments, are listed in Table 3.

Table 3: Effect of Aptamers on the Rate Constants for uPA Inhibition by PAI-1[a]

aptamer	k_{lim} (s^{-1})	K_m (μM)	k_{lim}/K_m (M^{-1} s^{-1})
none	8.90 ± 0.53 (3)	1.18 ± 0.37 (3)	(0.81 ± 0.25) × 10^7 (3)
paionap-5	5.72 ± 0.65 (3)[b]	0.32 ± 0.06 (3)[b]	(1.85 ± 0.57) × 10^7 (3)
paionap-40	3.69 ± 0.39 (3)[b]	0.21 ± 0.14 (3)[b]	(2.33 ± 1.43) × 10^7 (3)

[a]A stopped-flow fast kinetic analysis was performed to determine the rate of RCL insertion during the reaction of PAI-1$_{P9\text{-}NBD}$ with uPA. The reaction of PAI-1$_{P9\text{-}NBD}$ (10 nM) with different concentrations of uPA was followed, using excitation at 480 nm and measuring emission at 527 nm. Averaged k_{obs} values from 6 to 10 acquisitions at each uPA concentration were plotted vs the uPA concentration (Figure 5). k_{lim} and K_m values were estimated by fitting the data to eq 4. The table shows means and standard deviations from three independent experiments. [b]Significantly different from the corresponding value for PAI-1 alone ($p < 0.01$).

of the two aptamers caused almost complete protection against bis-ANS.

Effects of RNA Aptamers on the Binding of the uPA−PAI-1 Complex to LRP-1A and VLDLR. Having established that paionap-5, but not paionap-40, binds with high affinity to the uPA−PAI-1 complex, we were able to investigate the

Table 4: Effect of RNA Aptamers on the Rate of Conversion of PAI-1 to the Latent State[a]

	$t_{1/2}$ (min)			
PAI-1 variant	no addition	paionap-5	paionap-40	control aptamer[b]
E. coli	49 ± 16 (6)	192 ± 80 (4)[c]	398 ± 83 (3)[c]	50 ± 16 (3)
HT-1080	91 ± 26 (3)	165 ± 36 (3)[c]	716 ± 265 (3)[c]	86 ± 13 (3)

[a]Either of the two PAI-1 variants (11 nM) was incubated with or without aptamers (13 nM) at 37 °C. At various time points, samples were taken for the determination of specific inhibitory activity. The half-lives for latency transition were determined by semilogarithmic plots of the specific inhibitory activity vs incubation time. Means, standard deviations, and numbers of determinations are given. [b]The control aptamer was an aptamer clone from the library that did not bind PAI-1. [c]Significantly different from the half-life of PAI-1 alone ($p < 0.01$).

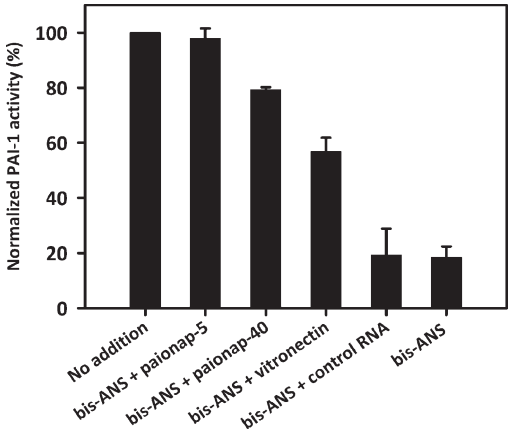

FIGURE 7: Effect of bis-ANS on the specific inhibitory activity of PAI-1 in the absence and presence of RNA aptamers. The specific inhibitory activity of PAI-1 was determined in the absence or presence of bis-ANS after preincubation with aptamers or vitronectin as indicated. The specific inhibitory activity of PAI-1 at each condition was expressed as a percentage of the specific inhibitory activity in the absence of additions. Means and standard deviations of three independent experiments are given.

effect of the aptamers on the binding of the uPA−PAI-1 complex to the clathrin-coated pit-localized endocytosis receptors LRP-1A and VLDLR. Both receptors bind the uPA−PAI-1 complex with a K_D of ~1 nM (*7*, *38*). We used an assay in which either of the two receptors was coated onto the solid phase of a 96-well Maxisorp microtiter plate and the complex added to the fluid phase in ^{125}I-labeled form. We added paionap-5 or paionap-40 at

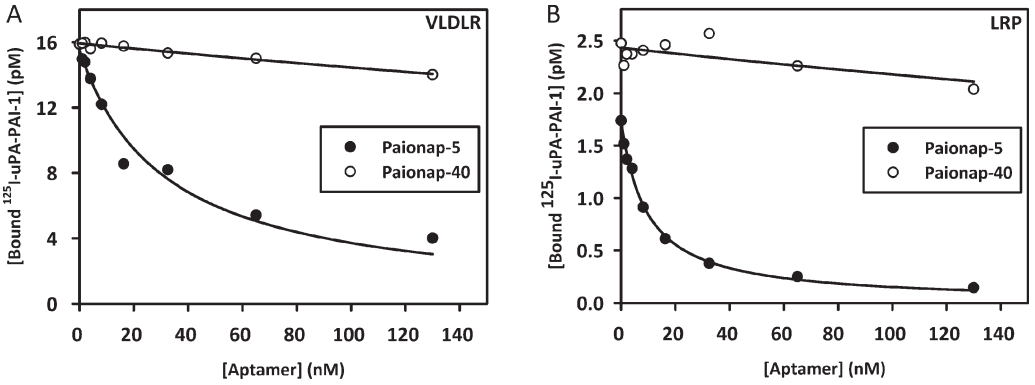

FIGURE 8: Effect of PAI-1 binding aptamers on the binding of the uPA−PAI-1 complex to endocytosis receptors. LRP (A) or VLDLR (B) was coated onto the solid phase of a 96-well plate. The binding of 20 pM [^{125}I]uPA−PAI-1 complex to the receptors was monitored in the presence of the indicated concentrations of paionap-5 (●) or paionap-40 (○). Each of the experiments shown represents a typical one of four independent experiments. The concentration of bound complex was plotted vs the free aptamer concentration. K_D values for binding of aptamers to the uPA−PAI-1 complex were determined by fitting the data to eq 5. Values of $(5.5 \pm 2.6) \times 10^{-9}$ ($n = 3$) and $(5.4 \pm 2.0) \times 10^{-9}$ M ($n = 5$) were obtained with LRP and VLDLR, respectively.

various concentrations between 0 and 130 nM. paionap-5 inhibited the binding of the [^{125}I]uPA−PAI-1 complex, while there was little effect of paionap-40 even at concentrations of up to 130 nM (Figure 8). Assuming that paionap-5 binding and receptor binding are mutually exclusive, a K_D value for binding of paionap-5 to the complex can be estimated by fitting the dependence of bound complex on the aptamer concentration to eq 5. Values of 2−8 nM at 4 °C were obtained, in good agreement with the values determined by SPR.

Effects of Aptamers in Cell Cultures. We further tested the effect of the aptamers on receptor-mediated endocytosis in U937 cells. These cells express uPAR which binds uPA and the uPA−PAI-1 complex with a K_D of ~100 pM and also express VLDLR (*50*). Endocytosis is dependent on an initial binding of the complex to uPAR, as the endocytosis receptors bind the complex inefficiently from the fluid phase (*8*). To assess endocytosis, we incubated the cells with the complex for 2 h and estimated the fraction of degraded complex by precipitation of the non-degraded complex with trichloroacetic acid. As controls, we first demonstrated inhibition of degradation by ATF of uPA, blocking the binding to uPAR, and by receptor-associated protein, blocking the binding to VLDLR. paionap-5, but not paionap-40, inhibited the degradation with an IC_{50} of ~100 nM (Figure 9).

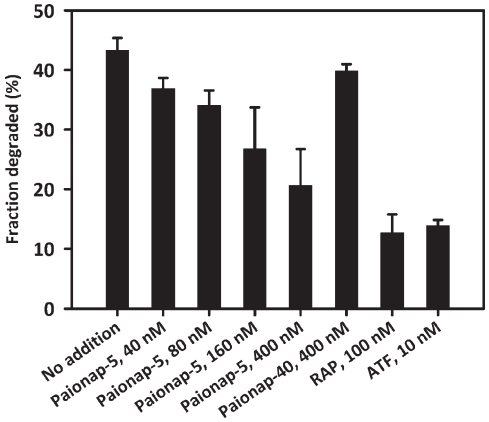

FIGURE 9: Effect of PAI-1 binding aptamers on receptor-mediated endocytosis of the uPA−PAI-1 complex. The [^{125}I]uPA−PAI-1 complex was preincubated with the indicated additions prior to addition to the U937 cells. The preincubated mixtures were then added to 1 mL aliquots containing 10^6 U937 cells, with a final [^{125}I]uPA−PAI-1 complex concentration of 10 pM, with 10 nM ATF, 100 nM RAP, 40−400 nM paionap-5, or 400 nM paionap-40. After incubation for 2 h at 37 °C in serum-free medium, the fraction of degraded complex was determined by addition of trichloroacetic acid. The bars show the means and standard deviations of the percentage of degraded complex from three independent experiments.

DISCUSSION

Aptamers recognizing a broad range of protein targets, including blood coagulation factors, growth factors, and extracellular matrix proteins, have been isolated in recent years. Such aptamers can potentially be used in the development of therapeutic formulations and diagnostic assays (*20*). One aptamer (NX 1838, Macugen, or pegaptanib sodium), inhibiting receptor binding of vascular endothelial growth factor (*51*), has been approved by the U.S. Food and Drug Administration for the treatment of age-related macular degeneration. Aptamers bind their targets with high affinity and high specificity. Accordingly, it has also become relevant to investigate the binding of aptamers to serpins. Recently, Blake et al. (*52*) reported the isolation of a PAI-1 binding RNA aptamer, with a binding site overlapping with that of vitronectin, and suggested that it can be used to inhibit the tumor biological functions of PAI-1. However, a much needed biochemical characterization of the aptamer was not undertaken.

We here describe a detailed biochemical characterization of binding and functional effects of two newly isolated PAI-1 binding aptamers, paionap-5 and paionap-40, and several observations of general interest concerning serpin structure and function as well as the possibility of pharmacological intervention with the pathophysiological effects of PAI-1. None of the aptamers inhibited the antiproteolytic effect of PAI-1, but both affected the binding of PAI-1 to vitronectin and the endocytosis receptors, as well as the conformational stability of PAI-1.

Footprinting analysis showed that the protein-binding elements of the aptamers are located in the aptamers' central, variable parts and largely consist of single-stranded loop regions, possibly folding into a specific structure upon binding to PAI-1. The flexibility of these regions allows a very close and specific interaction between RNA and protein. It is interesting to notice that the contact area of paionap-40 was larger than that of paionap-5, corresponding to the implication of more PAI-1 residues in the binding area for paionap-40 than in that for paionap-5. The restriction of the binding area largely to the variable region of the RNA suggests that it may

be possible to use aptamers of reduced length while maintaining binding strength.

A mutational screen identified the binding sites for both aptamers as being in the flexible joint region of PAI-1. A number of natural and synthetic ligands bind in this area (for reviews, see refs *2* and *3*). Thus, the N-terminal somatomedin B domain of vitronectin binds to residues centered around Arg103 and Gln125 in β-strand 2A and β-strand 1A, respectively (Figure 1) (*21*, *53*). An area centered on the top of α-helix E and the bottom of α-helix D forms an additional contact to vitronectin outside the somatomedin B domain (*43*). Vitronectin causes a 1.5−2-fold decrease in the latency transition rate and binds active PAI-1 with an affinity ~100-fold higher than that of the loop-inserted forms of PAI-1 (for reviews, see refs *2* and *3*). Some monoclonal antibodies (*54*) and a peptide (*55*), which bind to the loop connecting α-helix D and β-strand 2A, have a relatively low affinity for the active form of PAI-1 but a stronger affinity for latent PAI-1 and cause a strong to moderate increase in the latency transition rate. A number of small organochemical compounds, for instance, bis-ANS, have been shown to induce PAI-1 substrate behavior followed by conversion to a polymeric, likewise inactive state. These compounds bind to a hydrophobic pocket lined by α-helix D and β-strand 2A and have a differential affinity for active and loop-inserted forms of PAI-1 (for reviews, see refs *18* and *56*). Thus, each of these compounds responds to RCL insertion by a change in their binding affinity, when binding to the native form, that either delays or stimulates RCL insertion. There is bidirectional communication between the flexible joint region and the movements of the RCL. The differential effects of the ligands are coupled to different binding sites within the flexible joint region.

Since both aptamers impose functional effects on PAI-1 resembling those of vitronectin, i.e., prolongation of the latency transition half-life, delay of loop insertion during the reaction with target proteases, and protection against inactivation of PAI-1's antiproteolytic activity by organochemical compounds like bis-ANS (*48*, *57*−*59*), it is particularly instructive to compare their binding sites. The binding site for vitronectin is centered around Arg103 and Gln125, in β-strand 2A and β-strand 1A, respectively (*21*, *53*). Four residues, relatively close to each other at the bottom of α-helix D and the top of α-helix E, form the binding site for paionap-5. paionap-40 binds to the same four residues but, in addition, has a remarkable contact with Lys124. Interestingly, Lys124 is of little importance for the binding to vitronectin (*21*). Comparing the three-dimensional structures of active (*60*) and loop-inserted (*61*) forms of PAI-1, we can account for the ~100-fold lower affinity of somatomedin B for RCL-inserted PAI-1 than for active PAI-1 by relative large translocations of the side chains of the central binding residues, Arg103 and Gln125. In the aptamer binding sites, the four residues common to the binding sites for the two aptamers move relatively little upon RCL insertion (*60*, *61*), explaining the approximately identical affinities of paionap-5 for the two forms of PAI-1. However, the very weak binding of paionap-40 to the RCL-inserted forms of PAI-1 can be explained by a substantial relocation of Lys124 during loop insertion (*59*−*61*).

The differential binding sites for somatomedin B and each of the two aptamers are correlated with differential effects on the rate of conversion of PAI-1 to the latent state. First, it is remarkable that the latency transition of PAI-1 may be delayed by the aptamers, which have binding sites different from that of somatomedin B. Second, it is remarkable that paionap-40 causes the strongest delay of the PAI-1 latency transition ever reported for a specific ligand. Via comparison of the binding sites for paionap-5 and paionap-40, it seems clear that it is the contact of paionap-40 with Lys124 that enables this aptamer to delay the latency transition so strongly. Also, the aptamers seem to affect the movements of the RCL differently, as indicated by their different effects on the rate of inactivation of PAI-1 by the RCL-mimicking peptide TVASS. paionap-5 caused a small but significant acceleration of the inactivation of PAI-1 by TVASS. According to a recent report (*47*), such a change would suggest that the RCL goes from a partially inserted state to fully exposed state, leaving a gap between β-strands 3A and 5A open for incorporation of TVASS. In contrast, paionap-40 caused a severalfold deceleration of the rate of TVASS-induced inactivation, suggesting that its effect on the latency transition state has a mechanism completely different from that of paionap-5. The most ready explanation is that paionap-40 causes a complete extraction of the RCL but, in contrast to paionap-5, also a complete closure of the gap between β-strands 3A and 5A. The assumption that both aptamers cause a change in the RCL conformation agrees with the observation that both aptamers cause an increase in the second-order rate constant for the interaction between uPA and PAI-1, presumably resulting from a more optimal presentation of the RCL to the active site of the protease. In contrast, the effect on the k_{lim} for the reaction was modest, emphasizing the differential nature of strand insertion during complex formation and latency transition.

In agreement with the fact that only paionap-5 binds with high affinity to the RCL-inserted forms of PAI-1, this aptamer is an effective inhibitor of the binding of the uPA−PAI-1 complex to the endocytosis receptors LRP-1A and VLDLR. Endocytosis receptors of the low-density lipoprotein receptor family are responsible for the clearance of a variety of proteins from cell surfaces and the circulation (for a review, see ref *5*). Prominent among these proteins are plasminogen activator−serpin complexes (for a review, see ref *2*). The receptor binding area on the uPA−PAI-1 complex was mapped to an extended surface spanning both PAI-1 and uPA (*6*, *7*, *50*). On the PAI-1 moiety, the binding area encompasses the flexible joint region around α-helix D and α-helix E (*50*, *62*, *63*). paionap-5 binds exactly in this area. We previously isolated a PAI-1 binding cyclic peptide also binding in that area and also inhibiting endocytosis receptor binding (*64*). However, the IC_{50} for the peptide was in the micromolar range, so high that the window between the target specific effect and nonspecific detergent-like effects was very small. In contrast, the IC_{50} for paionap-5, as described here, is in the nanomolar range with no measurable effect of aptamers of irrelevant sequence.

Glycosylated PAI-1 has a slightly lower affinity for paionap-5 and paionap-40 than nonglycosylated PAI-1. The glycans attached to Asn211 of PAI-1 probably partly shield the binding sites. In agreement with this, we previously reported that PAI-1 variants lacking this glycosylation site have an increased affinity for monoclonal antibodies binding to the adjacent loop connecting α-helix D and β-strand 2A (*65*).

A variety of compounds have previously been isolated and characterized with respect to their effect on the various molecular interactions of PAI-1. Prominent among those are monoclonal antibodies developed to inhibit the antiproteolytic effect of PAI-1. They do so either by sterically hindering the access of plasminogen activators to the RCL, by inhibiting protease translocation, or by accelerating the conversion of PAI-1 to the inactive latent

state (for a review, see ref *66*). As mentioned above, a variety of organochemical compounds have been shown to induce PAI-1 substrate behavior followed by conversion to a polymeric, likewise inactive state (for reviews, see refs *18* and *56*). Common to these compounds is the fact that they inhibit more than one function of PAI-1. Compounds inhibiting the antiproteolytic effect will also inhibit the interaction with the endocytosis receptors, as PAI-1 in a complex with protease bind with higher affinity than free PAI-1 to these receptors. All the antiproteolytically inactive forms of PAI-1, induced by antibodies or organochemicals, bind to vitronectin with a drastically reduced affinity, and the substrate behavior-inducing antibodies compete with vitronectin for binding. In fact, paionap-40 is the first compound to be developed which among the three types of intermolecular interactions of PAI-1 has been demonstrated to inhibit only vitronectin binding. Compared to the organochemicals, the aptamers have the same advantages as the antibodies, having a high specificity and a high affinity. In conclusion, aptamers like those described here hold the promise of being useful for target validation in analysis of the molecular mechanisms of physiological and pathophysiological functions of PAI-1 in in vivo model systems. Furthermore, they will be useful tools for analyzing serpin conformational changes in in vitro studies.

ACKNOWLEDGMENT

Michael Ploug, the Finsen laboratory, is thanked for the gift of uPAR. Dr. R. Sousa (University of Texas Health Science Center) is thanked for providing us with an *E. coli* strain expressing the T7 RNA polymerase Y639F mutant.

REFERENCES

1. Huntington, J. A. (2006) Shape-shifting serpins: Advantages of a mobile mechanism. *Trends Biochem. Sci. 31*, 427–435.
2. Dupont, D. M., Madsen, J. B., Kristensen, T., Bodker, J. S., Blouse, G. E., Wind, T., and Andreasen, P. A. (2009) Biochemical properties of plasminogen activator inhibitor-1. *Front. Biosci. 14*, 1337–1361.
3. Wind, T., Hansen, M., Jensen, J. K., and Andreasen, P. A. (2002) The molecular basis for anti-proteolytic and non-proteolytic functions of plasminogen activator inhibitor type-1: Roles of the reactive centre loop, the shutter region, the flexible joint region and the small serpin fragment. *Biol. Chem. 383*, 21–36.
4. Andreasen, P. A., Egelund, R., and Petersen, H. H. (2000) The plasminogen activation system in tumor growth, invasion, and metastasis. *Cell. Mol. Life Sci. 57*, 25–40.
5. Gliemann, J., Nykjaer, A., Petersen, C. M., Jorgensen, K. E., Nielsen, M., Andreasen, P. A., Christensen, E. I., Lookene, A., Olivecrona, G., and Moestrup, S. K. (1994) The multiligand α2-macroglobulin receptor/low density lipoprotein receptor-related protein (α2MR/LRP). Binding and endocytosis of fluid phase and membrane-associated ligands. *Ann. N.Y. Acad. Sci. 737*, 20–38.
6. Jensen, J. K., Dolmer, K., and Gettins, P. G. (2009) Specificity of binding of the low density lipoprotein receptor-related protein to different conformational states of the clade E serpins plasminogen activator inhibitor-1 and proteinase nexin-1. *J. Biol. Chem. 284*, 17989–17997.
7. Nykjaer, A., Moller, B., Todd, R. F., III, Christensen, T., Andreasen, P. A., Gliemann, J., and Petersen, C. M. (1994) Urokinase receptor. An activation antigen in human T lymphocytes. *J. Immunol. 152*, 505–516.
8. Nykjaer, A., Petersen, C. M., Moller, B., Jensen, P. H., Moestrup, S. K., Holtet, T. L., Etzerodt, M., Thogersen, H. C., Munch, M., and Andreasen, P. A.; et al. (1992) Purified α2-macroglobulin receptor/LDL receptor-related protein binds urokinase·plasminogen activator inhibitor type-1 complex. Evidence that the α2-macroglobulin receptor mediates cellular degradation of urokinase receptor-bound complexes. *J. Biol. Chem. 267*, 14543–14546.
9. Durand, M. K., Bodker, J. S., Christensen, A., Dupont, D. M., Hansen, M., Jensen, J. K., Kjelgaard, S., Mathiasen, L., Pedersen, K. E., Skeldal, S., Wind, T., and Andreasen, P. A. (2004) Plasminogen activator inhibitor-I and tumour growth, invasion, and metastasis. *Thromb. Haemostasis 91*, 438–449.
10. Booth, N. A. (1999) Fibrinolysis and thrombosis. *Best Pract. Res., Clin. Haematol. 12*, 423–433.
11. Huber, K., Christ, G., Wojta, J., and Gulba, D. (2001) Plasminogen activator inhibitor type-1 in cardiovascular disease. Status report 2001. *Thromb. Res. 103* (Suppl. 1), S7–S19.
12. Vaughan, D. E. (2002) Angiotensin and vascular fibrinolytic balance. *Am. J. Hypertens. 15*, 3S–8S.
13. Erickson, L. A., Fici, G. J., Lund, J. E., Boyle, T. P., Polites, H. G., and Marotti, K. R. (1990) Development of venous occlusions in mice transgenic for the plasminogen activator inhibitor-1 gene. *Nature 346*, 74–76.
14. Eren, M., Painter, C. A., Atkinson, J. B., Declerck, P. J., and Vaughan, D. E. (2002) Age-dependent spontaneous coronary arterial thrombosis in transgenic mice that express a stable form of human plasminogen activator inhibitor-1. *Circulation 106*, 491–496.
15. Andreasen, P. A., Kjoller, L., Christensen, L., and Duffy, M. J. (1997) The urokinase-type plasminogen activator system in cancer metastasis: a review. *Int. J. Cancer 72*, 1–22.
16. Janicke, F., Prechtl, A., Thomssen, C., Harbeck, N., Meisner, C., Untch, M., Sweep, C. G., Selbmann, H. K., Graeff, H., and Schmitt, M. (2001) Randomized adjuvant chemotherapy trial in high-risk, lymph node-negative breast cancer patients identified by urokinase-type plasminogen activator and plasminogen activator inhibitor type 1. *J. Natl. Cancer Inst. 93*, 913–920.
17. Look, M. P., van Putten, W. L., Duffy, M. J., Harbeck, N., Christensen, I. J., Thomssen, C., Kates, R., Spyratos, F., Ferno, M., Eppenberger-Castori, S., Sweep, C. G., Ulm, K., Peyrat, J. P., Martin, P. M., Magdelenat, H., Brunner, N., Duggan, C., Lisboa, B. W., Bendahl, P. O., Quillien, V., Daver, A., Ricolleau, G., Meijer-van Gelder, M. E., Manders, P., Fiets, W. E., Blankenstein, M. A., Broet, P., Romain, S., Daxenbichler, G., Windbichler, G., Cufer, T., Borstnar, S., Kueng, W., Beex, L. V., Klijn, J. G., O'Higgins, N., Eppenberger, U., Janicke, F., Schmitt, M., and Foekens, J. A. (2002) Pooled analysis of prognostic impact of urokinase-type plasminogen activator and its inhibitor PAI-1 in 8377 breast cancer patients. *J. Natl. Cancer Inst. 94*, 116–128.
18. Andreasen, P. A. (2007) PAI-1: A potential therapeutic target in cancer. *Curr. Drug Targets 8*, 1030–1041.
19. Wilson, D. S., and Szostak, J. W. (1999) In vitro selection of functional nucleic acids. *Annu. Rev. Biochem. 68*, 611–647.
20. Pestourie, C., Tavitian, B., and Duconge, F. (2005) Aptamers against extracellular targets for in vivo applications. *Biochimie 87*, 921–930.
21. Jensen, J. K., Wind, T., and Andreasen, P. A. (2002) The vitronectin binding area of plasminogen activator inhibitor-1, mapped by mutagenesis and protection against an inactivating organochemical ligand. *FEBS Lett. 521*, 91–94.
22. Munch, M., Heegaard, C. W., and Andreasen, P. A. (1993) Interconversions between active, inert and substrate forms of denatured/refolded type-1 plasminogen activator inhibitor. *Biochim. Biophys. Acta 1202*, 29–37.
23. Hansen, M., Busse, M. N., and Andreasen, P. A. (2001) Importance of the amino-acid composition of the shutter region of plasminogen activator inhibitor-1 for its transitions to latent and substrate forms. *Eur. J. Biochem. 268*, 6274–6283.
24. Blouse, G. E., Perron, M. J., Kvassman, J. O., Yunus, S., Thompson, J. H., Betts, R. L., Lutter, L. C., and Shore, J. D. (2003) Mutation of the highly conserved tryptophan in the serpin breach region alters the inhibitory mechanism of plasminogen activator inhibitor-1. *Biochemistry 42*, 12260–12272.
25. Andreasen, P. A., Riccio, A., Welinder, K. G., Douglas, R., Sartorio, R., Nielsen, L. S., Oppenheimer, C., Blasi, F., and Dano, K. (1986) Plasminogen activator inhibitor type-1: Reactive center and amino-terminal heterogeneity determined by protein and cDNA sequencing. *FEBS Lett. 209*, 213–218.
26. Wind, T., Jensen, J. K., Dupont, D. M., Kulig, P., and Andreasen, P. A. (2003) Mutational analysis of plasminogen activator inhibitor-1. *Eur. J. Biochem. 270*, 1680–1688.
27. Shore, J. D., Day, D. E., Francis-Chmura, A. M., Verhamme, I., Kvassman, J., Lawrence, D. A., and Ginsburg, D. (1995) A fluorescent probe study of plasminogen activator inhibitor-1. Evidence for reactive center loop insertion and its role in the inhibitory mechanism. *J. Biol. Chem. 270*, 5395–5398.
28. Egelund, R., Petersen, T. E., and Andreasen, P. A. (2001) A serpin-induced extensive proteolytic susceptibility of urokinase-type plasminogen activator implicates distortion of the proteinase substrate-binding pocket and oxyanion hole in the serpin inhibitory mechanism. *Eur. J. Biochem. 268*, 673–685.
29. Kasza, A., Petersen, H. H., Heegaard, C. W., Oka, K., Christensen, A., Dubin, A., Chan, L., and Andreasen, P. A. (1997) Specificity of serine proteinase/serpin complex binding to very-low-density lipoprotein

receptor and α2-macroglobulin receptor/low-density-lipoprotein-receptor-related protein. *Eur. J. Biochem. 248*, 270–281.
30. Kenan, D. J., and Keene, J. D. (1999) In vitro selection of aptamers from RNA libraries. *Methods Mol. Biol. 118*, 217–231.
31. Grodberg, J., and Dunn, J. J. (1988) ompT encodes the *Escherichia coli* outer membrane protease that cleaves T7 RNA polymerase during purification. *J. Bacteriol. 170*, 1245–1253.
32. Zawadzki, V., and Gross, H. J. (1991) Rapid and simple purification of T7 RNA polymerase. *Nucleic Acids Res. 19*, 1948.
33. Zuker, M. (2003) Mfold web server for nucleic acid folding and hybridization prediction. *Nucleic Acids Res. 31*, 3406–3415.
34. Mathews, D. H., Sabina, J., Zuker, M., and Turner, D. H. (1999) Expanded sequence dependence of thermodynamic parameters improves prediction of RNA secondary structure. *J. Mol. Biol. 288*, 911–940.
35. Bodker, J. S., Wind, T., Jensen, J. K., Hansen, M., Pedersen, K. E., and Andreasen, P. A. (2003) Mapping of the epitope of a monoclonal antibody protecting plasminogen activator inhibitor-1 against inactivating agents. *Eur. J. Biochem. 270*, 1672–1679.
36. Vlassov, V. V., Giege, R., and Ebel, J. P. (1981) Tertiary structure of tRNAs in solution monitored by phosphodiester modification with ethylnitrosourea. *Eur. J. Biochem. 119*, 51–59.
37. Futamura, A., and Gettins, P. G. (2000) Serine 380 (P14) → glutamate mutation activates antithrombin as an inhibitor of factor Xa. *J. Biol. Chem. 275*, 4092–4098.
38. Heegaard, C. W., Simonsen, A. C., Oka, K., Kjoller, L., Christensen, A., Madsen, B., Ellgaard, L., Chan, L., and Andreasen, P. A. (1995) Very low density lipoprotein receptor binds and mediates endocytosis of urokinase-type plasminogen activator-type-1 plasminogen activator inhibitor complex. *J. Biol. Chem. 270*, 20855–20861.
39. Lund, L. R., Georg, B., Nielsen, L. S., Mayer, M., Dano, K., and Andreasen, P. A. (1988) Plasminogen activator inhibitor type 1: Cell-specific and differentiation-induced expression and regulation in human cell lines, as determined by enzyme-linked immunosorbent assay. *Mol. Cell. Endocrinol. 60*, 43–53.
40. Simonsen, A. C., Heegaard, C. W., Rasmussen, L. K., Ellgaard, L., Kjoller, L., Christensen, A., Etzerodt, M., and Andreasen, P. A. (1994) Very low density lipoprotein receptor from mammary gland and mammary epithelial cell lines binds and mediates endocytosis of M_r 40,000 receptor associated protein. *FEBS Lett. 354*, 279–283.
41. Berkenpas, M. B., Lawrence, D. A., and Ginsburg, D. (1995) Molecular evolution of plasminogen activator inhibitor-1 functional stability. *EMBO J. 14*, 2969–2977.
42. Jensen, J. K., Durand, M. K., Skeldal, S., Dupont, D. M., Bodker, J. S., Wind, T., and Andreasen, P. A. (2004) Construction of a plasminogen activator inhibitor-1 variant without measurable affinity to vitronectin but otherwise normal. *FEBS Lett. 556*, 175–179.
43. Schar, C. R., Blouse, G. E., Minor, K. H., and Peterson, C. B. (2008) A deletion mutant of vitronectin lacking the somatomedin B domain exhibits residual plasminogen activator inhibitor-1-binding activity. *J. Biol. Chem. 283*, 10297–10309.
44. Shore, J. D., Day, D. E., Francis-Chmura, A. M., Verhamme, I., Kvassman, J., Lawrence, D. A., and Ginsburg, D. (1995) A fluorescent probe study of plasminogen activator inhibitor-1. Evidence for reactive center loop insertion and its role in the inhibitory mechanism. *J. Biol. Chem. 270*, 5395–5398.
45. Schulze, A. J., Baumann, U., Knof, S., Jaeger, E., Huber, R., and Laurell, C. B. (1990) Structural transition of α1-antitrypsin by a peptide sequentially similar to β-strand s4A. *Eur. J. Biochem. 194*, 51–56.
46. Xue, Y., Bjorquist, P., Inghardt, T., Linschoten, M., Musil, D., Sjolin, L., and Deinum, J. (1998) Interfering with the inhibitory mechanism of serpins: Crystal structure of a complex formed between cleaved plasminogen activator inhibitor type 1 and a reactive-centre loop peptide. *Structure 6*, 627–636.
47. Li, S. H., Gorlatova, N. V., Lawrence, D. A., and Schwartz, B. S. (2008) Structural differences between active forms of plasminogen activator inhibitor type 1 revealed by conformationally sensitive ligands. *J. Biol. Chem. 283*, 18147–18157.
48. Egelund, R., Einholm, A. P., Pedersen, K. E., Nielsen, R. W., Christensen, A., Deinum, J., and Andreasen, P. A. (2001) A regulatory hydrophobic area in the flexible joint region of plasminogen activator inhibitor-1, defined with fluorescent activity-neutralizing ligands. Ligand-induced serpin polymerization. *J. Biol. Chem. 276*, 13077–13086.
49. Pedersen, K. E., Einholm, A. P., Christensen, A., Schack, L., Wind, T., Kenney, J. M., and Andreasen, P. A. (2003) Plasminogen activator inhibitor-1 polymers, induced by inactivating amphipathic organochemical ligands. *Biochem. J. 372*, 747–755.
50. Skeldal, S., Larsen, J. V., Pedersen, K. E., Petersen, H. H., Egelund, R., Christensen, A., Jensen, J. K., Gliemann, J., and Andreasen, P. A. (2006) Binding areas of urokinase-type plasminogen activator-plasminogen activator inhibitor-1 complex for endocytosis receptors of the low-density lipoprotein receptor family, determined by site-directed mutagenesis. *FEBS J. 273*, 5143–5159.
51. Ruckman, J., Green, L. S., Beeson, J., Waugh, S., Gillette, W. L., Henninger, D. D., Claesson-Welsh, L., and Janjic, N. (1998) 2′-Fluoropyrimidine RNA-based aptamers to the 165-amino acid form of vascular endothelial growth factor (VEGF165). Inhibition of receptor binding and VEGF-induced vascular permeability through interactions requiring the exon 7-encoded domain. *J. Biol. Chem. 273*, 20556–20567.
52. Blake, C. M., Sullenger, B. A., Lawrence, D. A., and Fortenberry, Y. M. (2009) Antimetastatic potential of PAI-1-specific RNA aptamers. *Oligonucleotides 19*, 117–128.
53. Zhou, A., Huntington, J. A., Pannu, N. S., Carrell, R. W., and Read, R. J. (2003) How vitronectin binds PAI-1 to modulate fibrinolysis and cell migration. *Nat. Struct. Biol. 10*, 541–544.
54. Verhamme, I., Kvassman, J. O., Day, D., Debrock, S., Vleugels, N., Declerck, P. J., and Shore, J. D. (1999) Accelerated conversion of human plasminogen activator inhibitor-1 to its latent form by antibody binding. *J. Biol. Chem. 274*, 17511–17517.
55. Mathiasen, L., Dupont, D. M., Christensen, A., Blouse, G. E., Jensen, J. K., Gils, A., Declerck, P. J., Wind, T., and Andreasen, P. A. (2008) A peptide accelerating the conversion of plasminogen activator inhibitor-1 to an inactive latent state. *Mol. Pharmacol. 74*, 641–653.
56. Vincenza Carriero, M., Franco, P., Vocca, I., Alfano, D., Longanesi-Cattani, I., Bifulco, K., Mancini, A., Caputi, M., and Stoppelli, M. P. (2009) Structure, function and antagonists of urokinase-type plasminogen activator. *Front. Biosci. 14*, 3782–3794.
57. Declerck, P. J., De Mol, M., Alessi, M. C., Baudner, S., Paques, E. P., Preissner, K. T., Muller-Berghaus, G., and Collen, D. (1988) Purification and characterization of a plasminogen activator inhibitor 1 binding protein from human plasma. Identification as a multimeric form of S protein (vitronectin). *J. Biol. Chem. 263*, 15454–15461.
58. Komissarov, A. A., Andreasen, P. A., Bodker, J. S., Declerck, P. J., Anagli, J. Y., and Shore, J. D. (2005) Additivity in effects of vitronectin and monoclonal antibodies against α-helix F of plasminogen activator inhibitor-1 on its reactions with target proteinases. *J. Biol. Chem. 280*, 1482–1489.
59. Blouse, G. E., Dupont, D. M., Schar, C. R., Jensen, J. K., Minor, K. H., Anagli, J. Y., Gardsvoll, H., Ploug, M., Peterson, C. B., and Andreasen, P. A. (2009) Interactions of Plasminogen Activator Inhibitor-1 with Vitronectin Involve an Extensive Binding Surface and Induce Mutual Conformational Rearrangements. *Biochemistry 48*, 1723–1735.
60. Sharp, A. M., Stein, P. E., Pannu, N. S., Carrell, R. W., Berkenpas, M. B., Ginsburg, D., Lawrence, D. A., and Read, R. J. (1999) The active conformation of plasminogen activator inhibitor 1, a target for drugs to control fibrinolysis and cell adhesion. *Structure 7*, 111–118.
61. Jensen, J. K., and Gettins, P. G. (2008) High-resolution structure of the stable plasminogen activator inhibitor type-1 variant 14-1B in its proteinase-cleaved form: a new tool for detailed interaction studies and modeling. *Protein Sci. 17*, 1844–1849.
62. Rodenburg, K. W., Kjoller, L., Petersen, H. H., and Andreasen, P. A. (1998) Binding of urokinase-type plasminogen activator-plasminogen activator inhibitor-1 complex to the endocytosis receptors α2-macroglobulin receptor/low-density lipoprotein receptor-related protein and very-low-density lipoprotein receptor involves basic residues in the inhibitor. *Biochem. J. 329* (Part 1), 55–63.
63. Horn, I. R., van den Berg, B. M., Moestrup, S. K., Pannekoek, H., and van Zonneveld, A. J. (1998) Plasminogen activator inhibitor 1 contains a cryptic high affinity receptor binding site that is exposed upon complex formation with tissue-type plasminogen activator. *Thromb. Haemostasis 80*, 822–828.
64. Jensen, J. K., Malmendal, A., Schiott, B., Skeldal, S., Pedersen, K. E., Celik, L., Nielsen, N. C., Andreasen, P. A., and Wind, T. (2006) Inhibition of plasminogen activator inhibitor-1 binding to endocytosis receptors of the low-density-lipoprotein receptor family by a peptide isolated from a phage display library. *Biochem. J. 399*, 387–396.
65. Gils, A., Pedersen, K. E., Skottrup, P., Christensen, A., Naessens, D., Deinum, J., Enghild, J. J., Declerck, P. J., and Andreasen, P. A. (2003) Biochemical importance of glycosylation of plasminogen activator inhibitor-1. *Thromb. Haemostasis 90*, 206–217.
66. Gils, A., and Declerck, P. J. (2004) The structural basis for the pathophysiological relevance of PAI-I in cardiovascular diseases and the development of potential PAI-I inhibitors. *Thromb. Haemostasis 91*, 425–437.